MHD simulations of the post-adiabatic SNRs in the interstellar magnetic field

O. Petruk[1,2], T. Kuzyo[1], V. Beshley[1,3]

[1]Institute for Applied Problems in Mechanics and Mathematics (Lviv, Ukraine)
[2]INAF-Osservatorio Astronomico di Palermo (Italy)
[3]Astronomical Observatory, National University (Lviv, Ukraine)

Introduction

Typical picture of supernova remnant (SNR) evolution consists of the three stages — free expansion, adiabatic and radiative — each with its own features. It is often assumed that these phases change one another very rapidly comparing to the duration of the phases themselves. However, the transition from the fully adiabatic to the fully radiative shock lasts almost the same time as duration of the adiabatic stage [9]. It has its own, different from other stages, features [2]. First, the presence of the dynamically important radiative losses does not allow the Sedov (1959) model to be used. Second, the thin cold radiative shell has not formed yet and, therefore, the solution for the radiative shock [1,7,8] is not relevant. Therefore, there is the need to consider separately the post-adiabatic stage in a general scenario of the SNR evolution. This is of importance especially in SNRs interacting with molecular clouds.
Hydrodynamic properties of the post-adiabatic flows are demonstrated in the numerical simulations [2,3]. There is an approximate semi-analytical method to describe the post-adiabatic SNR [4].
Here, the evolution of the post-adiabatic SNRs in the interstellar medium with magnetic field (MF) is presented. We solve numerically the system of differential equations of the ideal MHD in order to see how does MF affect the evolution of the post-adiabatic SNRs.

Numerical simulations

The numerical code PLUTO [5,6] is adopted for our simulations. It is designed to describe the supersonic flows in the presence of strong shocks. PLUTO integrates the system of the time-dependent conservation laws of the ideal MHD in the form

$$\frac{\partial}{\partial t}\begin{pmatrix}\rho\\ \mathbf{m}\\ E\\ \mathbf{B}\end{pmatrix}+\nabla\cdot\begin{pmatrix}\rho\mathbf{v}\\ \mathbf{m}\mathbf{v}-\mathbf{B}\mathbf{B}+\mathbf{I}p_{\rm tot}\\ (E+p_{\rm tot})\mathbf{v}-\mathbf{B}(\mathbf{v}\cdot\mathbf{B})\\ \mathbf{v}\mathbf{B}-\mathbf{B}\mathbf{v}\end{pmatrix}^{\rm T}=\begin{pmatrix}0\\ 0\\ L\\ 0\end{pmatrix} \quad (1)$$

where ρ is the density, $\mathbf{m}=\rho\mathbf{v}$ the momentum density, $\mathbf{v}$ the flow velocity, $p_{\rm tot}$ the total (thermal p and magnetic $p_{\rm B}$) pressure, $\mathbf{I}$ the unit vector, $\mathbf{B}$ the MF strength, L represents the radiative losses, E the total energy density. The ideal gas equation of state is assumed with $\gamma=5/3$. The total energy density is a sum of the thermal, kinetic and magnetic components:

$$E=\frac{p}{\gamma-1}+\frac{m^2}{2\rho}+\frac{B^2}{2}. \quad (2)$$

Additionally, the divergence-free condition holds: $\nabla\cdot\mathbf{B}=0$.
We used:

- the following configuration of the numerical simulations: linear interpolation with min mod limiter, HLL Riemann solver and Characteristic Tracing algorithm for the time evolution;
- the eight wave formulation for controlling $\nabla\cdot\mathbf{B}=0$ condition;
- one-dimensional spherically-symmetrical model;
- the physical grid size is 32 pc with 60 000 computational zones.

Effect of MF on evolution of the post-adiabatic SNRs

MF affects the evolution of the shock. Fig. 1: the shock radius R, velocity V (**a**), expansion parameter m (**b**) for *parallel and perpendicular shocks*, and the energy components (**c, d**).

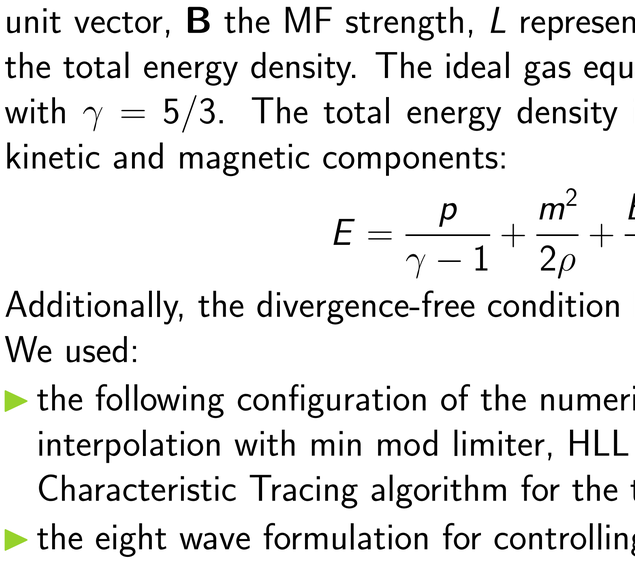

Figure 1: Effect of magnetic field on the dynamics of shock with radiative losses.
R, V (**a**); m (**b**)
$B_o=0\,\mu$G and $B_\parallel$ (red),
$B_{o\perp}=3$ (blue), 10 (green) and 30 μG (orange) .
$B_{o\perp}=10\,\mu$G (**c**),
$B_{o\perp}=30\,\mu$G (**d**).
$E_{\rm o}=10^{51}$ erg,
$n_{\rm o}=0.84$ cm^{-3}.

Effect of MF on hydrodynamic parameters of the flow

The tangential MF is an important factor in the dynamics of the post-adiabatic flows with shocks. Figs 2 and 3 show the time evolution of the spatial distributions of the temperature and density.

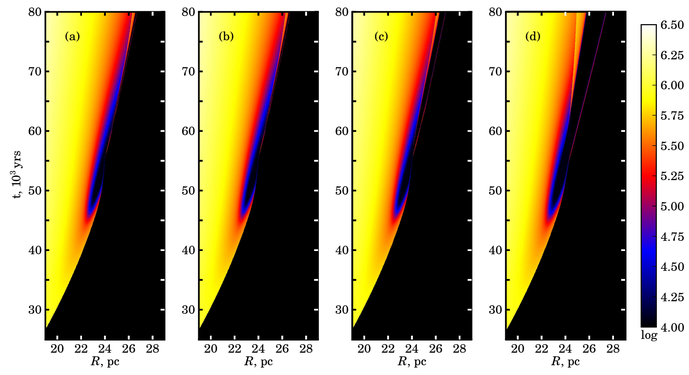

Figure 2: Time dependence of the distribution of temperature behind the shock. (**a**) $B_{\rm o}=0\,\mu$G, (**b**) $B_{\rm o\parallel}=3\,\mu$G, (**c**) $B_{\rm o\perp}=3\,\mu$G, (**d**) $B_{\rm o\perp}=10\,\mu$G. Color scale is the same for all plots (in Kelvin, logarithmic scale).

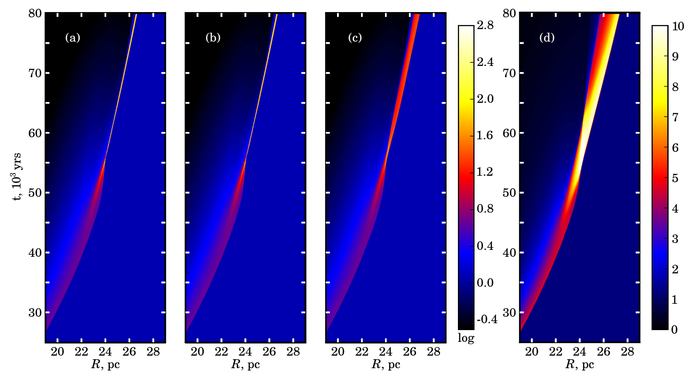

Figure 3: Time dependence of the distribution of the number density behind the shock. (**a**) $B_{\rm o}=0\,\mu$G, (**b**) $B_{\rm o\parallel}=3\,\mu$G, (**c**) $B_{\rm o\perp}=3\,\mu$G, (**d**) $B_{\rm o\perp}=10\,\mu$G. Color bar on the right of the plot (**c**) is for the three left plots (in cm^{-3}, logarithmic scale). Color bar on the right corresponds to the plot (**d**) (in cm^{-3}, linear scale).

Magnetic field tructure

The radial MF is not compressed behind the shock. MF parallel to the shock normal does not affect the flow structure during the entire evolution of SNR because its energy density is much smaller than the thermal energy density.
The distribution of tangential MF downstream of the post-adiabatic shock depends on the MF strength (Fig. 4).

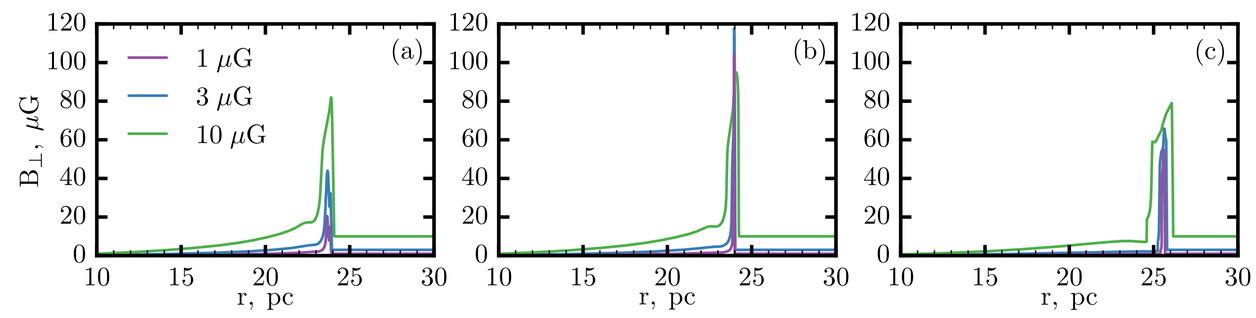

Figure 4: Radial profiles of the magnetic field downstream of the perpendicular shock. $t=53\,000$ yrs (**a**), $t=55\,000$ yrs (**b**), $t=70\,000$ yrs (**c**).

Conclusions

- Parallel MF does not affect the flow dynamic.
- The perpendicular MF provides a bit higher shock speed on the post-adiabatic stage.
- The radiative losses come mostly from the thermal energy component while MF takes energy mostly from the kinetic energy.
- The perpendicular MF limits the density jump in the thin radiative shell.
- The thickness of the radiative post-shock shell is larger for the perpendicular shock and the structure of the radiative shell is more smoothed for the perpendicular MF.
- These effects are more prominent for higher perpendicular MF.

References

[1] Bandiera R., Petruk O., 2004, A&A, 419, 419
[2] Blondin J. M. et al., 1998, ApJ, 500, 342
[3] Cioffi D. F. et al., 1988, ApJ, 334, 252
[4] Hnatyk B. et al., 2007, Kin. Phys. Celest. Bodies, 23, 137
[5] Mignone A. et al., 2007, ApJS, 170, 228
[6] Mignone A. et al., 2012, ApJS, 198, 7
[7] McKee C., Ostriker J., 1977, ApJ, 218, 148
[8] Pasko V., Silich S., 1986, Kin. Phys. Celest. Bodies, 2, 15
[9] Petruk O., 2005, Journal of Physical Studies, 9, 364
[10] Sedov L., 1959, Similarity and Dimensional Methods in Mechanics. Academic Press, New York

Acknowledgements

All simulations were performed on the computational cluster in Institute for Applied Problems in Mechanics and Mathematics. The research was partially supported by the Program of Ukrainian Academy of Science "Grid infrastructure and grid technologies for science and applications" (grant 0115U002936).